Cyclometalated platinum(II) complexes of 2,2'-bipyridine *N*-oxide containing 1,1'-bis(diphenylphosphino)ferrocene ligand: Structural, computational and electrochemical studies

Hamid R. Shahsavari,[a] Masood Fereidoonnezhad,[b,e*] Maryam Niazi,[a] S. Talaat Mosavi,[a] Sayed Habib Kazemi,[a] Reza Kia,[c]* Shima Shirkhan,[b] Siamak Abdollahi Aghdam[a] and Paul R. Raithby[d]*

[a]Department of Chemistry, Institute for Advanced Studies in Basic Sciences (IASBS), Yousef Sobouti Blvd., Zanjan 45137-6731, Iran.

[b]Department of Medicinal Chemistry, School of Pharmacy, Ahvaz Jundishapur University of Medical Sciences, Ahvaz, Iran.

[c]Chemistry Department, Sharif University of Technology, P.O. Box 11155-3516, Tehran, Iran.

[d]Department of Chemistry, University of Bath, Claverton Down, Bath, Avon BA2 7AY, United Kingdom.

[e]Cancer, Environmental and Petroleum Pollutants Research Center, Ahvaz Jundishapur University of Medical Sciences, Ahvaz, Iran.

Email: shahsavari@iasbs.ac.ir, fereidoonnezhad-m@ajums.ac.ir, rkia@sharif.edu

Abstract

The preparation and characterization of new heteronuclear-platinum(II) complexes containing 1,1'-bis(diphenylphosphino)ferrocene (dppf) ligand are described. The reaction of the known starting complex [PtMe(κ^2N,C-bipyO-H)(SMe_2)], **A**, in which bipyO-H is a cyclometalated "rollover" 2,2'-bipyridine *N*-oxide, with the dppf ligand in a 2 : 1 ratio or an equimolar ratio led to the formation of corresponding binuclear complex [Pt_2Me_2(κ^2N,C-bipyO-H)$_2$(μ-dppf)], **1**, or mononuclear complex [PtMe(κ^1C-bipyO-H)(dppf)], **2**, respectively. According to the reaction conditions, the dppf ligand in **1** and **2** behaves as either a bridging or chelateing ligand. All complexes were characterized by NMR spectroscopy. The solid-state structure of **2** was determined by single-crystal X-ray diffraction method and it was shown that the chelateing dppf ligand in this complex was arranged "synclinal-staggered" conformation. Also, the occurrence of

intermolecular $C–H_{Cp}\cdots O_{bipyO\text{-}H}$ interactions in the solid-state gave rise to an extended 1-D network. The electronic absorption spectra and the electrochemical behavior of these complexes are discussed. Density functional theory (DFT) was used for geometry optimization of the singlet states in solution and for electronic structure calculations. The analysis of the molecular orbital (MO) compositions in terms of occupied and unoccupied fragment orbitals in **2** was performed.

Introduction

Ever since the serendipitous synthesis of *ferrocene*, numerous derivatives have been prepared.[1, 2] In this regard, ferrocenyl phosphine compounds are a well-known family of ferrocene derivatives that are extensively used in organometallic and coordination chemistry.[1-3] One of the most important ferrocenyl phosphine compounds is 1,1'-bis(diphenylphosphino)ferrocene (dppf).[1, 2, 4] The dppf is a biphosphine ligand and can adopts numerous coordination modes in complexes of a range of transition metals.[1-18] These dppf complexes have been utilized in several area such as catalysis, materials science, electrochemistry, and biology.[1, 2, 7, 9, 10, 19-21]

On the other hand, the chemistry of cyclometalated complexes is of great interest because of their use in a wide range of applications.[22-26] For example, one of the most fascinating class of cyclometalated complexes is rollover category.[27-30] In this family, the cyclometalated moieties are bidentate heterocyclic donors (2,2'-bipyridine (bipy),[29] 2,2'-bipyridine *N*-oxide (bipyO)[31]) rather than classical monodentate ligands (2-phenylpyridine (ppy),[24] 2-vinylpyridine (vpy)[32, 33]). The bipyO ligand has been by far less explored than bipy ligand in rollover cycolmetalation[31] or in coordination chemistry.[34] The 2,2'-bipyridine *N*-oxide ligand has the two most important possible binding modes in coordination to different metals (Chart 1) which are related to the nature of central metal.[31, 34]

As part of our ongoing research into the cyclometalation chemistry of platinum,[32, 35-37] we now present the preparation and characterization of new neutral platinum(II) rollover complexes bearing the dppf as a spacer or chelating ligand. Furthermore optical and electrochemical properties of these complexes are described, the results being supported by theoretical calculations.

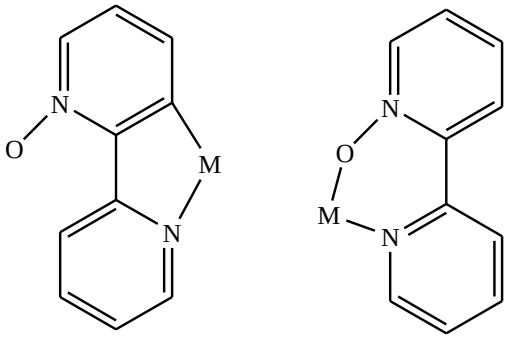

κ^2N,C κ^2N,O

Chart 1. The potential binding modes of 2,2'-bipyridine *N*-oxide ligand: left, bipyO-H mode and right, bipyO mode.

Result and discussion

Synthesis and characterization

The new chemistry to prepare of cycloplatinated(II) rollover complexes are depicted in Scheme 1.

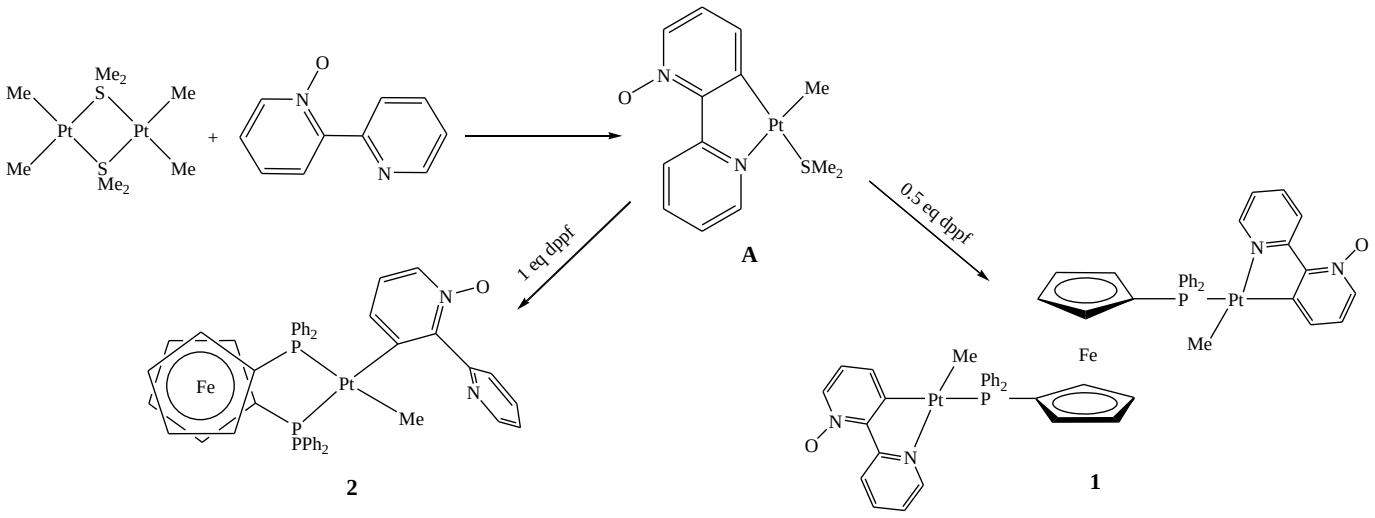

Scheme 1. The mononuclear and binuclear cycloplatinated(II) rollover complexes containing dppf ligand.

The precursor complex [PtMe(κ^2N,C-bipyO-H)(SMe_2)], **A**,[31] in which bipyO-H is a cyclometalated "rollover" 2,2'-bipyridine *N*-oxide, was prepared by the published method, by

reaction of the known dimeric dimethylplatinum(II) complex *cis,cis*-[$PtMe_2(\mu$-SMe2)$_2PtMe_2$][38] with 2 equivalents of 2,2'-bipyridine *N*-oxide in acetone. Complex **A** was reacted with 0.5 equivalent of 1,1'-bis(diphenylphosphino)ferrocene (dppf) ligand by replacement of the labile dimethyl sulfide ligand with the phosphorus donor atoms of the dppf ligand. This reaction afforded the binuclear complex [$Pt_2Me_2(\kappa^2N,C$-bipyO-H)$_2(\mu$-dppf)], **1**, which formed as a yellow precipitate. In this complex the dppf ligand adopts an "open bridge" conformation.[2, 5-10] However, when complex **A** was treated with one equivalent of the dppf ligand the Pt–$N_{bipyO-H}$ bond easily dissociated, and the mononuclear complex [PtMe(κ^1C-bipyO-H)(dppf)], **2**, was formed. This bond breaking is related to the potent chelating ability of dppf ligand due to its large P^P bite angle.[2] A similar bond cleavage reaction has been observed in analogues cycloplatinated(II) complexes.[6, 10, 31, 39-41] Complexes **1** and **2** are air-stable and obtained in high yields. They are soluble in halogenated solvents such as CH_2Cl_2 or $CHCl_3$ and stable for several days at room temperature in the solution.

Complexes **1** and **2** were characterized by elemental analyses and their integrity in solution was confirmed by multinuclear NMR spectroscopy (^{1}H, ^{31}P and ^{195}Pt ($CDCl_3$)), more details are collected in the Experimental Section. The schematic labeling for complexes is shown in Scheme 2.

The structure of binuclear complex **1** was established firstly by ^{1}H NMR spectroscopy (Figure S1). In complex **1** the equivalent methyl signal (δ = 0.90 ppm) is split into a doublet by the ^{31}P nucleus ($^3J_{PH}$ = 7.2 Hz) and there is also splitting of the signal from the ^{195}Pt nucleus ($^2J_{PtH}$ = 82.2 Hz). The platinum coupling constant value confirms that the Me groups are located *trans* to the nitrogen atoms rather than *trans* to the phosphorus atoms.[6, 8] Also, the observation of a single methylplatinum signal confirms that the two PtMe(bipyO-H) moieties are equivalent.[6, 8] Another useful piece of evidence for confirming of this equivalency was the observation of only one low field signal for each of the two $H^{3'}$ (δ = 9.91 ppm) or H^6 (δ = 8.11 ppm) protons of the pyridyl ring of bipyO-H ligands.[6-8, 31] Moreover, the uncommon chemical shift observed for the $H^{3'}$ proton is dependent on the orientation of this proton toward the *N*-oxide (N–O) group.[31, 42] The two broad singlet resonances at δ = 4.39 and 4.30 can be assigned to the four α and β protons of the cyclopentadienyl moieties (Cp) of dppf ligand, respectively. This observation confirmed the

equivalency of the two Cp rings in the dppf ligand.[6-10] The $^{31}P\{^{1}H\}$ NMR spectrum of complex **1** (Figure S2) revealed only a singlet signal along with ^{195}Pt satellites at δ = 23.3 ppm with $^{1}J_{PtP}$ = 2307 Hz, which supports the assignment that both P atoms were equivalent and positioned *trans* to a coordinated carbon atom of cyclometalated ligand. The $^{195}Pt\{^{1}H\}$ NMR spectrum of complex **1** (Figure S3) displayed a doublet at δ = -4167 ppm with $^{1}J_{PtP}$ = 2316 Hz, which was close to obtained value from the $^{31}P\{^{1}H\}$ NMR spectrum. Additionally, these observations confirmed that the dppf ligand was symmetrically bridged between the two platinum centers.[6-10]

The ^{1}H NMR spectrum of complex **2** was particularly informative and in accordance with the suggested formulation (Figure S4). This spectrum exhibited a doublet of doublet resonance for Pt–Me protons at δ = 0.03 ppm which coupled to the platinum center ($^{2}J_{PtH}$ = 65.6 Hz) and to two different phosphorus atoms ($^{3}J_{PH}$ = 8.7 and 6.6 Hz) representing the *cis* and *trans* coupling constants to the P atoms.[6, 18] The platinum coupling constant value obtained for **2** was significantly lower than the observed value for **1** and confirmed the methyl ligand in complex **2** adopts the *trans* C–Pt–P arrangement. The *α* and *β* protons of the dppf ligand appeared as eight broad singlet signals between δ = 3.47-4.97, confirming all hydrogen atoms of the Cp rings are in different environments, *i.e.* the two Cp moieties are inequivalent. This pattern indicates that the dppf chelate is fairly rigid and adopts the staggered conformation.[2, 6] These data are consistent with the replacement of the nitrogen atom of cyclometalated ligand by means of dppf ligand and confirms the high chelating ability of this ligand.[2] The $^{31}P\{^{1}H\}$ NMR spectrum of complex **2** is shown in Figure 1, and confirmed the chelated coordination of dppf ligand. It displays two distinctive doublets at δ = 19.1 ppm and 23.6 ppm, assigned to the chemically different phosphorus atom donors, with platinum satellites of $^{1}J_{Pt-P}$ = 2191 Hz (P^{a} atom *trans* to the $\kappa^{1}C$-bipyO-H) and $^{1}J_{Pt-P}$ = 1959 Hz (P^{b} atom *trans* to the Me), respectively. This result indicates that the methyl ligand applied higher *trans* influence than the coordinated carbon atom of bipyO-H ligand.[6] As will be shown in the Structural Determination section, the Pt–P^{b} bond distance is somewhat longer than that of the Pt–P^{a} bond length. It is interesting to note that perhaps owing to the dppf ligand exerting more strain in its chelating form, the ^{195}Pt coupling constant value (P atom *trans* to the C atom of cyclometalated ligand) in **2** is noticeably lower than in **1** (acting as a bridging ligand).[6] Also, in **2** a *cis*-P–P coupling ($^{2}J_{P^{a}P^{b}}$ = 17.2 Hz) was detected, clearly confirming the two inequivalent

phosphorus atoms couple to each other through the platinum center.[6, 18] Consistent with the $^{31}P\{^{1}H\}$ NMR spectrum, in the $^{195}Pt\{^{1}H\}$ NMR spectrum (Figure S5) of **2**, a doublet of doublets was observed at δ = -4578 ppm with $^{1}J_{PtP}$ = 2193 Hz and 1968 Hz.

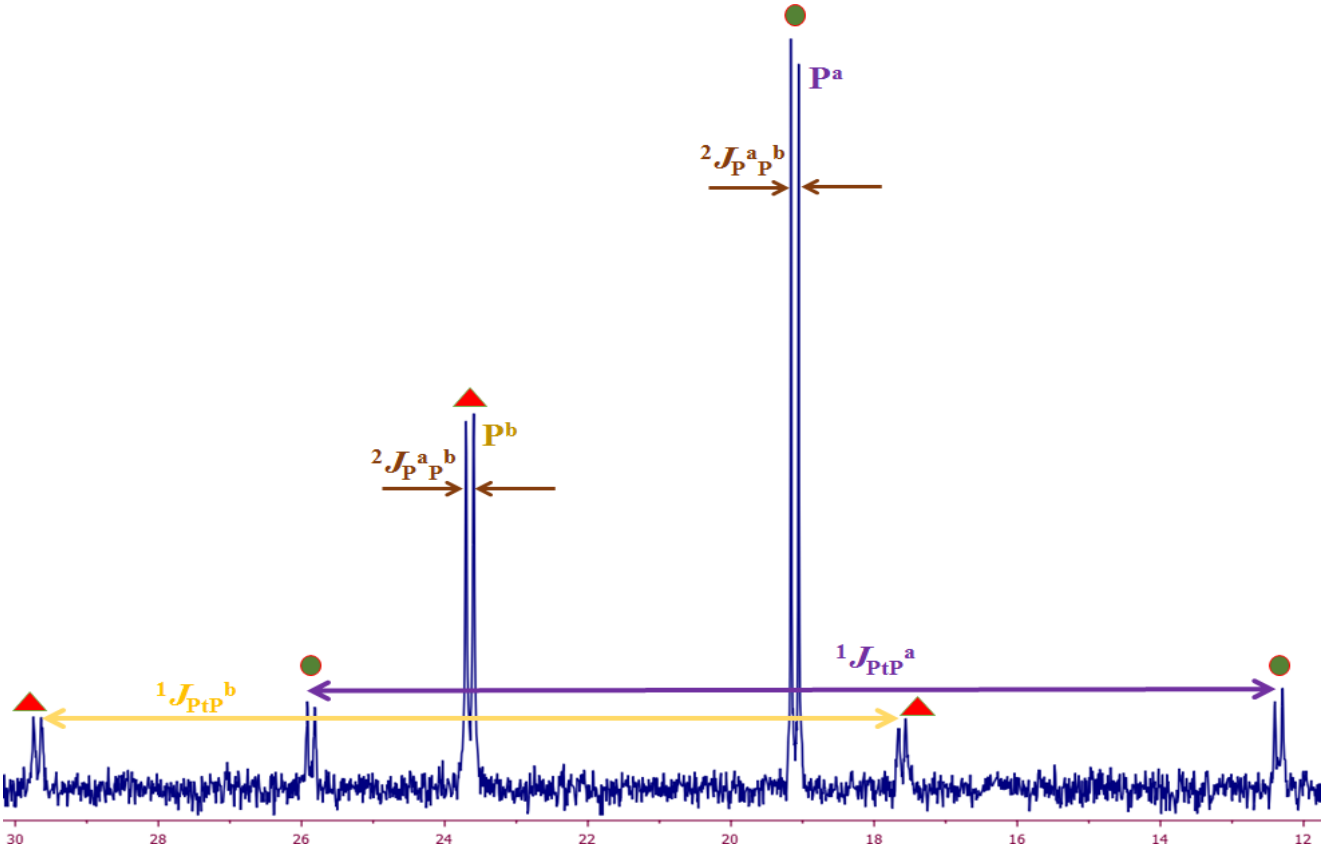

Figure 1. $^{31}P\{^{1}H\}$ NMR spectrum of complex **2** in $CDCl_3$ at room temperature.

Structural Determination

The structure of **2** was determined by X-ray crystallography and two views of the molecule are shown in Figure 2. Crystallographic data is summarized in Table S1. Complex **2** contains a square planar platinum(II) center with the methyl group, the *ortho* C of the bipyO-H ligand, and two P atoms of the dppf ligand acting as the coordinating atoms. The angles around the Pt center are rather close to the ideal angle of 90°, and this could be contrasted with the strain observed in, for example, organoplatinum complexes containing bis(diphenylphosphino)amine, dppa, as chelating ligand.[43]

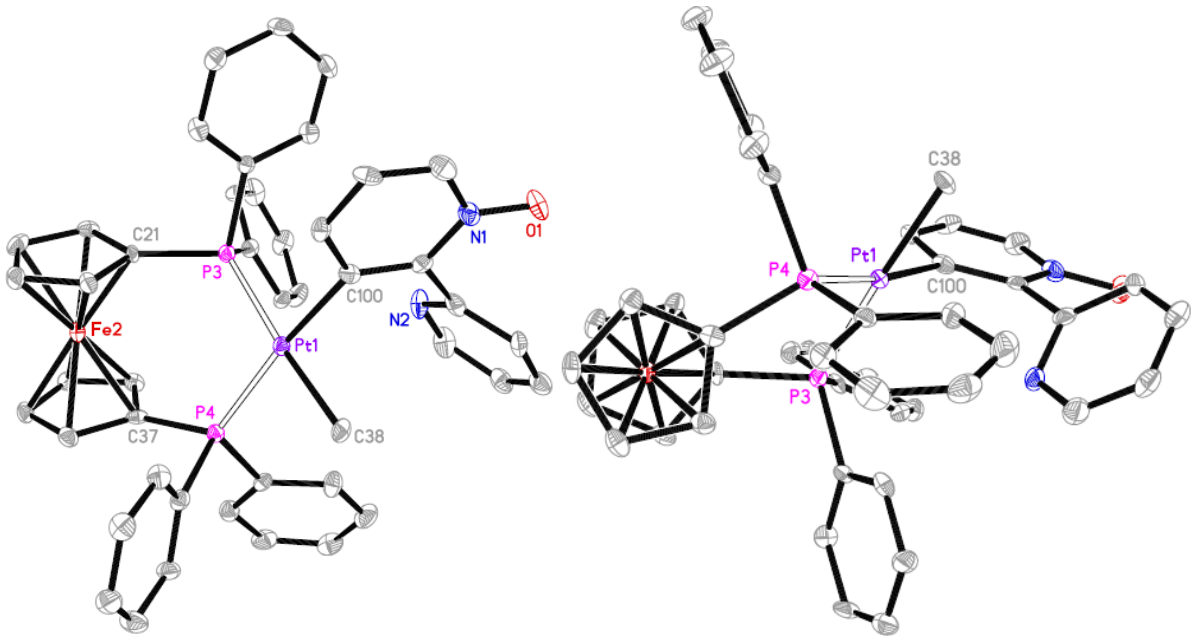

Figure 2. Two orientations of the unique molecule of **2**, as determined crystallographically, with thermal ellipsoids at the 40% probability level. Hydrogen atoms have been omitted for clarity. Pt(1)-C(100) 2.075(10), Pt(1)-C(38) 2.127(10), Pt(1)-P(3) 2.301(3), Pt(1)-P(4) 2.295(3), P(3)-C(21) 1.803(10), P(4)-C(37) 1.821(11), P(4)-Pt(1)-P(3) 97.96(10), C(100)-Pt(1)-C(38) 85.5(4), C(100)-Pt(1)-P(3) 89.7(3), C(100)-Pt(1)-P(4) 172.0(3), C(38)-Pt(1)-P(3) 175.2(3), C(38)-Pt(1)-P(4) 86.8(3).

The imine N is not coordinated and is positioned opposite to the platinum center, and this is in contrast to the usual preference of the bipyO-H ligand to form cyclometalated complexes.[31] The dppf ligand is arranged in the usually preferred synclinal-staggered conformation.[4] The Pt(1)-P(3) distance of 2.301(2) Å is longer than the Pt(1)-P(4) distance of 2.295(3) Å, indicating that the methyl ligand probably exerts a higher *trans* influence than the bipyO-κ^1C ligand.[31] This observation is in agreement with NMR spectroscopic data. On the other hand, the geometry around the metal center is also affected by the intramolecular $\pi\cdots\pi$ [3.670(6) Å] interaction of the pyridine-N-oxide segment and one of the phenyl rings of the dppf ligand.

The interesting feature of the crystal packing of complex **2** is connection of the neighboring molecules into a 1-D extended chain along the *a*-axis by the intermolecular C–H$\cdots$O [C14–H14A$\cdots$O1^{i}, (i) 1-x,-1/2+y,9/2-z and C22–H22A$\cdots$O1^{ii}, (ii) -1+x,y,z] hydrogen bonding (Figure 3).

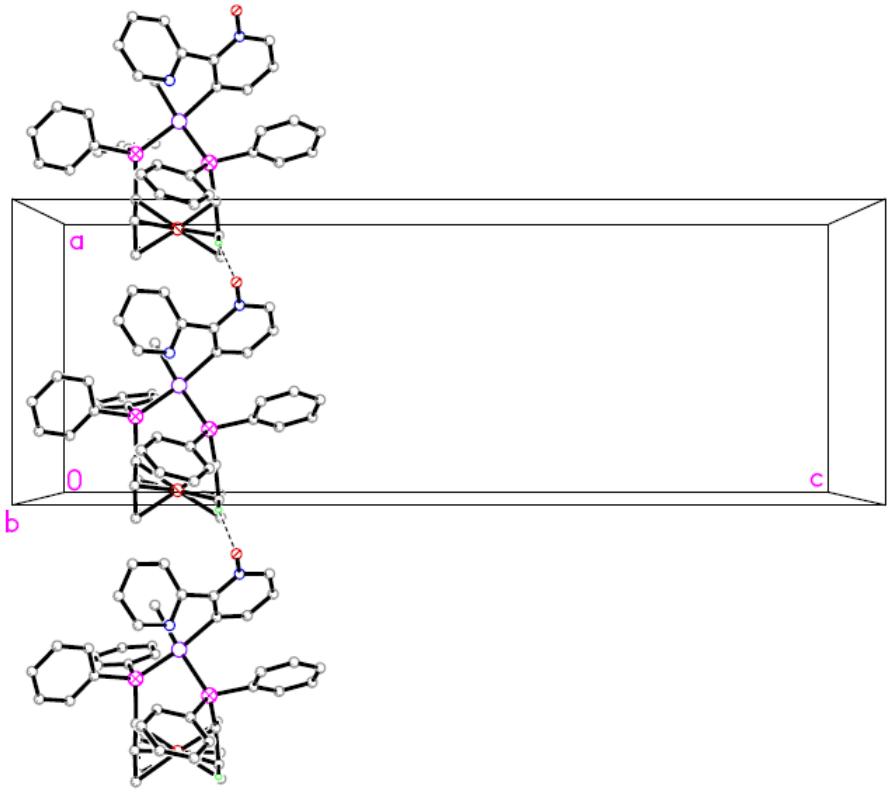

Figure 3. The crystal packing of **2** viewed down the *b*-axis showing 1-D extended chain along the *a*-axis by the intermolecular C–H···O interactions.

Optical properties

The UV-vis absorption spectra of all complexes **A**, **1** and **2** were obtained in CH_2Cl_2 at ambient temperature (Figure 4) and the data are summarized in Table S2. Also, the electronic absorption spectral data for the dppf ligand[3, 19] is included for comparison.

Complex **A** shows high energy and more intense transitions between 280-320 nm (Table S2). These transitions are attributable to the intraligand charge transfer transitions (^{1}ILCT, $\pi \rightarrow \pi^*$) located on the bipyO-H cyclometalated ligand which are slightly perturbed by coordination to the metal center.[10, 44] The less intense bands at 361 nm 388 and nm are assignable to mixed spin-allowed ^{1}IL and ^{1}MLCT transitions (metal to ligand charge transfer).[32, 44] The spectrum of dppf ligand displays two main absorption band (Table S2). The more intense band at higher energy (in the UV region) is due to $\pi \rightarrow \pi^*$ transition and the less intense visible absorption band is mostly due to ^{1}MLCT transition ($d(Fe^{II}) \rightarrow \pi^*$).[19, 45] Complexes **1** and **2** reveal two main bands with

different extinction coefficients (Table S2). The high energy band at UV region is remarkably intense and red shifted relative to that reported band for complex **A**. This profile can be ascribed to a $\pi \rightarrow \pi^*$ (^{1}ILCT) transition which is localized on the bipyO-H cyclometalated and the dppf ligands.[10, 19] While the low intensty bands (ε = 8.6-9.2 M^{-1} cm^{-1}) in the visible region for **1** are similar to complex **A** with slight red shift. Probably, this shift is associated to increasing of contribution of the ^{1}MLCT transition and dppf ligand has hardly any influence on these lower energy profiles (Figure 4).[10] However, in contrast, in **2** the less intense peaks (ε = 3.4-6.1 M^{-1} cm^{-1}) in this region are admixture transitions and are assignable to ^{1}L'LCT (ligand to ligand charge transfer, π bipyO-H $\rightarrow \pi^*$ dppf) with a minor contribution of ^{1}MLCT ($d(Pt^{II}) \rightarrow$ bipyO-H), an assignment which is supported by time-dependent DFT (TD-DFT) calculations (see below).

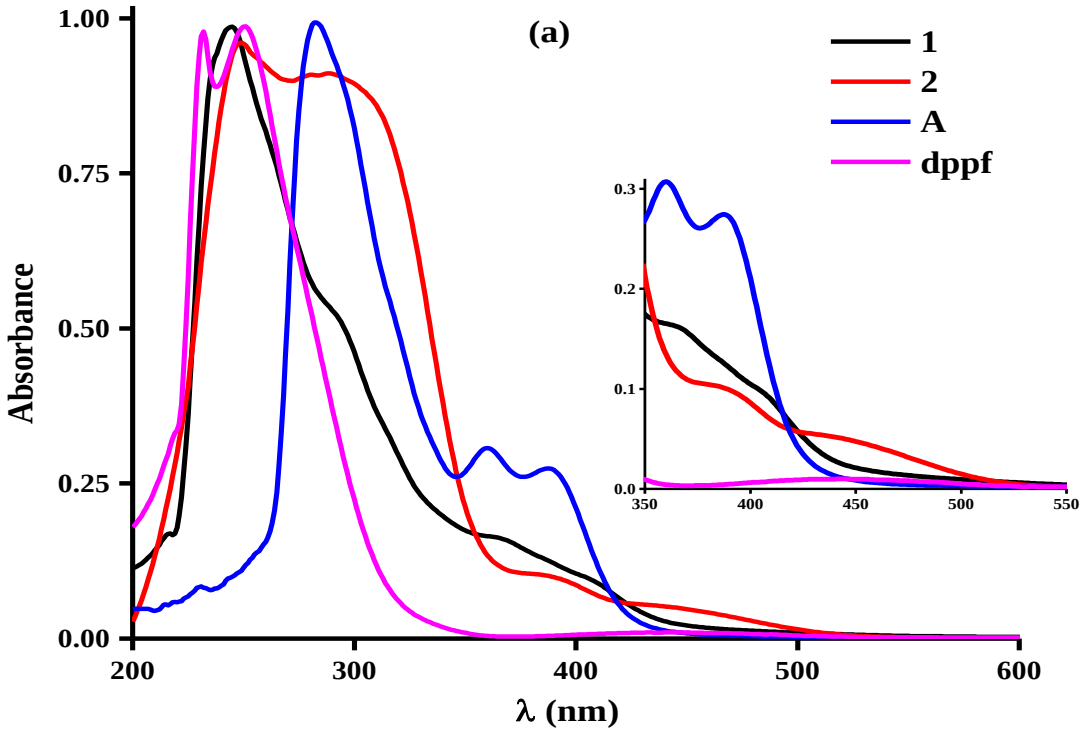

Figure 4. Electronic absorption spectra of complexes **A**, **1**, **2** and dppf ligand in CH_2Cl_2 solution (5×10^{-5}M) at room temperature (Inset: low energy region).

Computational studies

Electronic structure

The singlet state geometry of complex **2** was optimized in the gas phase using B3LYP functional of the Gaussian09 program package.[46] The molecular orbitals (MO) and singlet excited states of this complex were also studied. The data for the composition of the most important occupied and unoccupied molecular orbitals and the atomic orbital compositions for each complex (%) are listed in Table S3. The contour plots of the selected important frontier molecular orbitals of **2** are depicted in Figure S6. Because of the important role of the frontier molecular orbitals in the electronic excitations and the electronic transition characteristics, it will be useful to map the highest occupied (HOMO) and lowest unoccupied (LUMO) orbitals of **2** on the framework for the excited-state TD-DFT calculations. Therefore, **2** was divided to four segments: the platinum centre (Pt), the methyl group (Me), the bipyO-H cyclometalating ligand and the dppf ligand. Each part of the percentage contributions are the sum of the atomic orbital coefficient squares. The frontier molecular orbitals (5 occupied MOs and 5 unoccupied MOs) are listed according to their energy and the segment contribution. The assignment of each MO was made on the basis of its composition from the segments. The composition of the LUMO is localized on the dppf ligand (π^* character) but the HOMO orbital is mainly localized on the bipyO-H ligand. The HOMO – 1 and HOMO – 2 orbitals have significant contribution from Pt metal centre (Table S3).

Analysis of chemical bonding

(Extent of donation and back-donation by charge decomposition analysis)

The chemical bonding between the platinum center and the ligands in complex **2** can be explained on the basis of donation from the ligands to the metal and π-back-donation from the metal segment to the ligand(s) (σ-donation & π-back-donation) in terms of charge decomposition analysis (CDA) and extended charge decomposition analysis (ECDA).[47, 48] The CDA and Mulliken population analysis (MPA) studies were used to provide better qualitative and quantitative understanding of the chemical bonding in this complex. The procedure for calculating the contributions for each occupied molecular orbital of complex **2**: (i) charge donation through the combination of the occupied orbitals of the ligands and the unoccupied orbitals of the metal

segment which can be further split into σ and π donation, (ii) charge π-back-bonding through the combination of the occupied orbitals of the metal segment and the unoccupied orbitals (mostly π^*) of the ligand and (iii) electronic polarization of the metal segment and the ligand. The electronic polarization of fragments is due to the distortion of the electron distribution of the fragments on each other and includes the interactions between all permanent charges and charge multipoles and induced multipoles. The CDA gives reasonable estimates of donation and π-back-donation between the molecular segments only if there is no electronic polarization or it is significantly small. If it is not the case, the difference between the amount of the electron donation and back-donation will not be the same to the net charge transfer between the segments, as calculated from the sum of the atomic charges. Table 1 summarized some of the properties derived from the charge decomposition analysis of complex **2**. It can be noted from Table 1 that based on the quantitative data resulted from CDA calculations by AOMix 6.88 software the σ-donation character of the methyl group is greater than the bipyO-H ligand and this is in line to the stronger *trans* influence of the methyl group in lengthening of the opposite bond.

Table 1. Summary of computed properties of complex **2**.

Property	
%LUFO[a]$_{Pt}$ in OMOs[c]	89.16 (1.78 e)
%HOFO[b]$_{bipyO-H}$ in UMOs[d]	35.51 (0.71 e)
%HOFO$_{dppf}$ in UMOs	21.39 (0.43 e)
Donation (au); Me→Pt	0.71 e
Donation (au); bipyO-H→Pt	0.43 e
Donation (au); dppf→Pt	0.12 e
π-CT[e] (au); Pt→bipyO-H	0.05 e
π-CT (au); Pt→dppf	0.24 e

[a] LUFO = lowest unoccupied fragment orbital. [b] HOFO = highest occupied fragment orbital [c] OMOs = occupied molecular orbitals in the complex. [d] UMOs = unoccupied molecular orbitals in the complex. [e] π-Back-donation from the Pt fragment to L.

Calculated electronic absorption spectra

TD-DFT calculations were employed to examine the 50 low-lying singlet excited states of complex **2**. The overlay of the experimental and simulated UV-vis spectra of complex **2** is depicted in Figure S7. It can be seen that the simulated optical absorption spectra from the TD-DFT calculations reproduces the main features of the experimental spectra. Selected low-lying singlet

excited states together with their vertical excitation energies, oscillator strengths and assignment of the transitions for complex **2** is summarized in Table 2. The energy of each excited state is vertical excitation energy in electron volts from the ground state. The spectral assignment is on the basis of the comparison of experimental band maxima with calculated energies of the transitions with reasonable oscillator strengths. The excitation of an electron from an occupied to an unoccupied molecular orbital is an experimental model for the excited state (*i.e.,* a one-electron picture). However, the excited states calculated herein demonstrate that excited-state electronic structures are best described in terms of multi-configurations, wherein a linear combination of several occupied-to-unoccupied MO excitations comprises a given optical transition. Assignment of the character of each excited state was based on the compositions of the occupied and unoccupied MOs of the dominant configuration(s) for that excited state. The highest occupied molecular orbital (HOMO) of complex **2** contains contributions from the bipyO-H ligand (91.6% of *p* orbitals). The HOMO – 1 and HOMO – 2 are mainly located on the Pt and bipyO-H ligand. On the other hand, LUMO and LUMO + 1 have significant contribution from the dppf ligand. The low-energy calculated absorption band (437 nm) in complex **2** corresponds to excited state S_7. It is attributed to the charge transfer from the bipyO-H ligand to the dppf ligand and minor charge transfer from the Pt to the bipyO-H ligand (HOMO – 1 → LUMO contribution). The high-energy absorption band (251 nm) corresponds to excited state 39 and is attributed to the charge transfer from molecular orbitals which are mainly localized on the bipyO-H and the dppf ligands. Electron density difference maps (EDDMs) derived from the TD-DFT calculations were used to show the electron density changes between the ground and excited states upon different electronic excitations. It represents a way for visualizing the electronic distribution, for which one can subtract the ground-state electron density (S_0) from the Franck-Condon electron density of the excited state, thereby providing a picture of the redistribution of the electron density after the vertical transition from the ground-state to any of the Franck-Condon excited states. Visualization of these difference density plots can provide an insight into the subsequent geometric changes occurring on the excited-state potential energy surface, and to determine what type of excitation is occurring.[49, 50] The electron density difference maps (EDDMs) of complex **2** is shown in Figure 5, confirm the assignment of the calculated electronic transitions in Table 2.

Table 2. Selected TD-DFT calculated excitation energies and compositions of the lowest-lying singlet excited states for complex **2**.

States	E(eV)/λ(nm)	*f*	$\lambda_{exp.}$	Type	Assignment
7	3.92/437	0.05	449	HOMO → LUMO (71%)	LL'CT, MLCT
				HOMO – 1 → LUMO (9%)	
39	4.94/251	0.06	248	HOMO – 5 → LUMO + 1 (33%)	$\pi\rightarrow\pi^*$(IL)

H and **L** refer to the highest-occupied and lowest-unoccupied molecular orbitals, respectively.

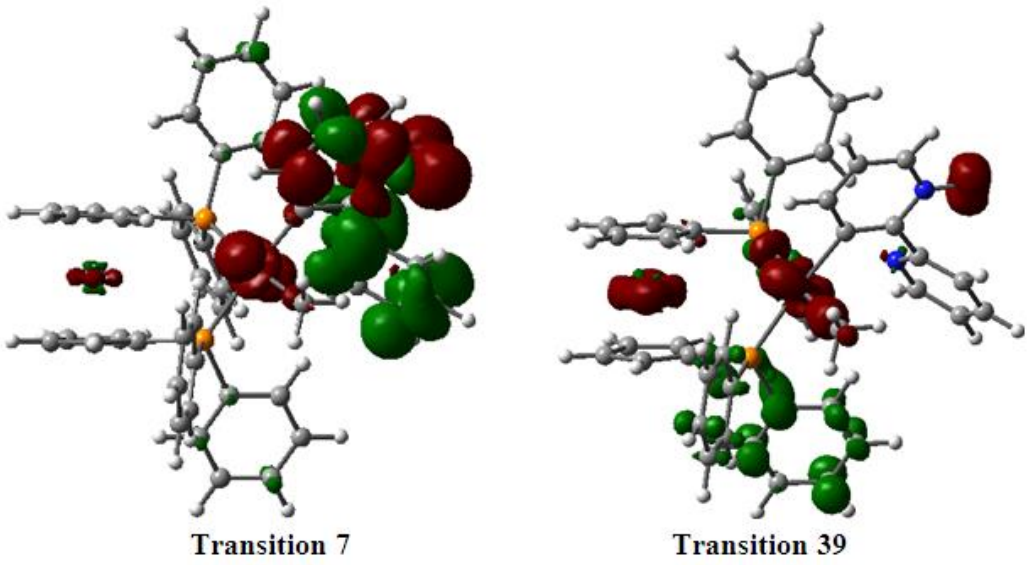

Figure 5. Electron density difference maps (EDDMs) for main transitions in complex **2**. Red indicates a decrease in charge transfer, while green indicates an increase.

Electrochemistry

The electrochemical behavior of the free dppf ligand and complexes **1**, **2**, [Pt_2Me_2(κ^2*N*,*C*-ppy)$_2$(μ-dppf)], **3**,[6] [PtMe(κ^1*C*-ppy)(dppf)], **4**,[6] in which ppy = 2-phenylpyridinyl, between -2.0 to +2.0 V *vs*. reference electrode at a scan rate of 5 mV s^{-1} is presented in Figure S8 (complexes **3** and **4** were selected for comparison purpose). Oxidation and reduction potentials of these complexes are also provided as Table S4.

The dppf ligand oxidation onset is around +0.5 V and the peak potential is approximately located at 1.25 V vs. Ag/AgCl.[19] Also, the cyclic voltammogram of the dppf ligand in acetonitrile shows almost irreversible kinetics in which a reduction peak was observed. The complexes containing dppf ligand in their structure were also investigated by cyclic voltammetry. As shown

in Figure S8, both complexes **1** and **2** show a pair of quasireversible oxidation and reduction peaks which can be assigned to the Pt redox activity. Of course, the oxidation peaks of the dppf ligand and Pt are overlapped but the reduction peaks appeared at approximately -1.25 V originated from the reduction of Pt. It was observed that the oxidation of Pt and the dppf ligand occurs at more positive potentials compared to free Pt or the dppf ligand. Moreover, cyclic voltammograms of complexes **3** and **4** revealed that the oxidation behavior of dppf ligand occurred at more positive potentials with lower peak currents compared to the free dppf ligand behavior. Additionally, a broad reduction wave was observed for both complexes around -1.0 V which can be attributed to the reduction of Pt. Detailed electrochemical studies of the dppf containing species in the narrower potential range were carried out and it was found that only complexes **1** and **3** display significant electrochemical activity in the range of -1.0 to +1.0 V. Figure 6 depicts the voltammograms of these two complexes.

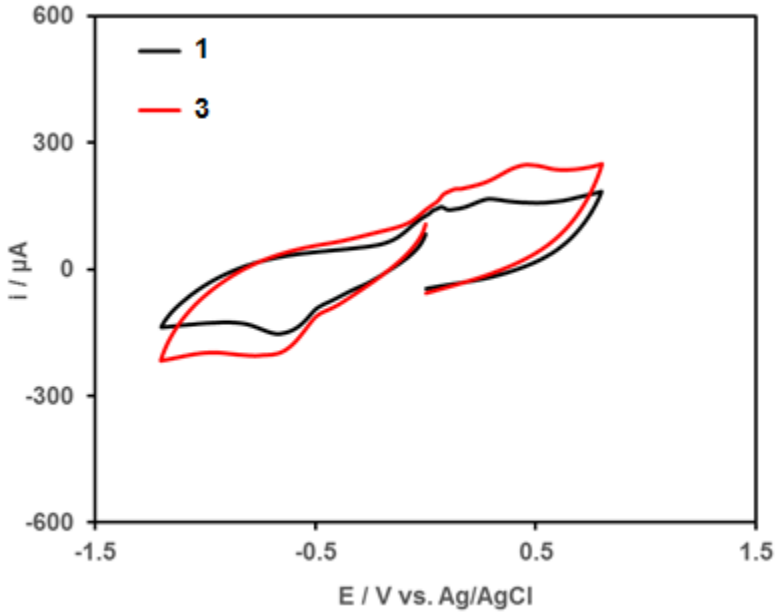

Figure 6. The cyclic voltammograms of complexes **1** and **3** in 0.05 M $LiClO_4$-Acetonitrile at a scan rate of 5 mV s^{-1}.

As seen in Figure S8, the voltammogram of complex **2** is similar to the electrochemical behavior of Pt electrode, which may indicate the lower interaction of Pt with the dppf ligand in this complex compared to complex **1**. It may suggests that the dppf group in the structure of

complex **2** does not have insignificant changes on its electrochemical behavior. Therefore, for **2** the electrochemistry is relatively similar to the Pt electrochemistry; and may indicate a lower stability of this complex and possible destruction of complex **2** under potential cycling during electrochemical studies. Of course, both complexes **1** and **2** show a broad peak of dppf but for the case of **1** redox peaks of ferrocene part (Fc) are more distinguishable. Perhaps, in complex **1**, the dppf ligand (particularly, the Fc part) becomes more available for electron transfer. On the other hand, the redox behavior of complex **3** is similar to complex **1**, especially as seen in Figure 6 in the potential range of -1.0 V to 1.0 V. The redox behavior of complexes **1**-**4** seems to be nearly independent of the bipyO-H or ppy groups on their structure.

Conclusion

Dppf is an excellent ligand for the development of molecular architecture with transition metals. The cycloplatinated complex **A** was smoothly reacted with the dppf ligand (in varying molar ratios) to produce different products due to the various coordinating abilities of this ligand. When 0.5 equivalent of the dppf ligand was used it acts as a spacer ligand and the dinuclear complex **1** was formed. In contrast, when one molar equivalent of this ligand was applied, the dppf easily displaced the bipyO-H nitrogen to provide the P^P chelated mononuclear complex **2**; this behavior is related to large bite angle of dppf. In the crystal structure of **2** the dppf ligand was found to has a synclinal-staggered conformation for the Cp rings. Moreover, this complex showed an interesting hydrogen bond interaction between $C–H_{Cp}\cdots O_{bipyO\text{-}H}$ (Figure 3) and generating a one-dimensional network structure in the solid-state. The platinum-phosphorus bond distance for phosphorus atom *trans* to the coordinated carbon atom of bipyO-H ligand was slightly shorter than the phosphorus atom *trans* to the methyl ligand. This difference suggests that the κ^1C-bipyO-H ligand perhaps exerted a lower *trans* influence than the Me ligand. Also, the charge decomposition analyses and molecular orbital diagrams revealed the nature of the compositions of the molecular orbitals of complex **2** based on the fragments analysis and charge donation and back-donation character of the coordinated ligand. These calculations were confirmed the greater *trans* influence of the Me ligand than the C atom of cyclometalating ligand in complex **2**. The UV-vis and electrochemical properties of these complexes have been investigated. The lower energy bands in **1** and **2** were assignable to mixed spin-allowed ^{1}IL/^{1}MLCT or ^{1}L'LCT/^{1}MLCT (which supported

by TD-DFT calculations), respectively. Complexes **1** and **2** displayed a pair of quasireversible oxidation and reduction peaks. They could be assigned to the platinum center and the dppf unit. These platinum complexes presented here could thus also potentially be biologically active and the screening of their anticancer behavior is currently under investigation.

Experimental

All NMR spectra (^{1}H, ^{31}P {^{1}H} and ^{195}Pt {^{1}H}) were recorded on a Brucker Avance DPX 400 MHz instrument. References were TMS or the residual peak of the solvent, *i.e.* $CDCl_3$ (^{1}H), 85% H_3PO_4 (^{31}P), and aqueous Na_2PtCl_6 (^{195}Pt). The chemical shifts (δ) were reported as ppm and coupling constants (*J*) expressed in Hz. The microanalyses were performed using a vario EL CHNS elemental analyzer. All solvents were purified and dried according to standard procedures.[51] 2,2'-bipyridine *N*-oxide and 1,1′-bis(diphenylphosphino)ferrocene were purchased from Aldrich. The precursor complex [PtMe(κ^2*N*,*C*-bipyO-H)(SMe_2)], **A**,[31] was prepared by the literature method. The NMR labeling for all ligands are shown in Scheme 2 for clarifying the chemical shift assignments.

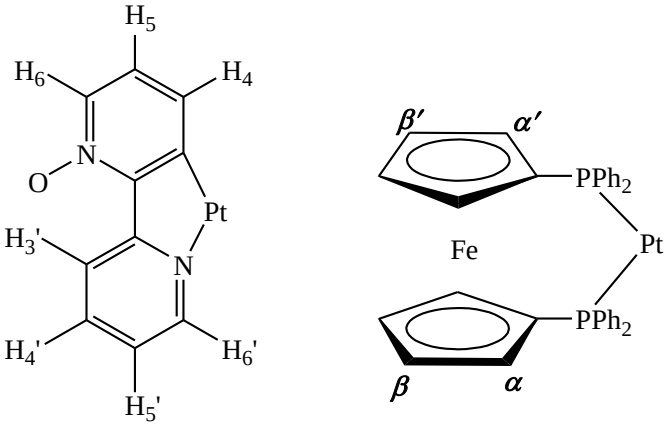

bipyO-H **dppf**

Scheme 2. Representative ligands with position labeling.

Synthesis of complexes

[Pt$_2$Me$_2$(κ^2N,C-bipyO-H)$_2$(μ-dppf)], 1

To a solution of complex **A** (100 mg, 0.22 mmol) in acetone (10 mL) was added 0.5 equivalent of dppf (62.5 mg, 0.11 mmol) and the solution was stirred for 2 h at room temperature. A yellow solid was participated which was separated and dried under vacuum. Yield: 68%, mp. = 253 ˚C. Anal. Calcd. For $C_{56}H_{48}FeN_4O_2P_2Pt_2$ (1317); C, 51.07; H, 3.67; N, 4.25. Found: C, 50.35; H, 3.51; N, 4.09. NMR data in $CDCl_3$: δ(^{1}H) 0.90 (d, $^2J_{PtH}$ = 82.2 Hz, $^3J_{PH}$ = 7.2 Hz, 6H, 2 Me groups), 4.30 (br s 4H, β and β' of Cp protons), 4.39 (br s, 4H, α and α' of Cp protons), 6.64 (t, $^3J_{HH}$ = 6.4 Hz, 2H, H$^{5'}$), 7.18 (t, $^3J_{HH}$ = 7.3 Hz, 2H, H^5), 7.33-7.40 (m, 8H, overlapping multiplets), 7.41-7.47 (m, 4H, overlapping multiplets), 7.60 (t, $^3J_{HH}$ = 7.4 Hz, 2H, H$^{4'}$), 7.63-7.75 (m, 8H, overlapping multiplets), 7.76-7.86 (m, 4H, overlapping multiplets), 8.11 (d, $^3J_{HH}$ = 6.2 Hz, 2H, H^6), 9.91 (d, $^3J_{HH}$ = 8.1 Hz, $^3J_{PtH}$ = 54.7 Hz, 2H, H$^{3'}$); δ(^{31}P) 23.3 (s, $^1J_{PtP}$ = 2307 Hz, 2P of dppf); δ(^{195}Pt) -4167 (d, $^1J_{PtP}$ = 2316, 2Pt).

[PtMe(κ^{1}C-bipyO-H)(dppf)], 2

To a solution of complex **A** (100 mg, 0.22 mmol) in acetone (10 mL) was added 1 equivalent of dppf (125 mg, 0.22 mmol) and the solution was stirred for 2 h at room temperature, which produced a yellow solution. After removing of the solvent under reduced pressure, the residue was treated with diethyl ether (2 × 3 mL). The precipitate as a yellow solid was dried under vacuum. Yield: 78%, mp. = 234 ˚C. Anal. Calcd. For $C_{45}H_{38}FeN_2OP_2Pt$ (936.7); C, 57.76; H, 4.09; N, 2.99. Found: C, 56.84; H, 3.69; N, 3.08. NMR data in $CDCl_3$: δ(^{1}H) 0.03 (dd, $^2J_{PtH}$ = 65.6 Hz, $^3J_{PH}$ = 8.7, 6.6 Hz, 3H, 1 Me group), 3.47, 3.53, 3.99 and 4.06 (each a br s, 4H, β and β' of Cp protons), 4.19, 4.31, 4.60 and 4.97 (each a br s, 4H, α and α' of Cp protons), 6.46 (t, $^3J_{HH}$ = 6.9 Hz 1H, H$^{5'}$), 7.01-7.21 (m, 6H, overlapping multiplets), 7.27-7.42 (m, 11H, overlapping multiplets), 7.45-7.52 (m, 3H, overlapping multiplets), 7.56-7.69 (m, 3H, overlapping multiplets), 7.71-7.79 (m, 2H, H^6, H$^{6'}$), 8.39 (d, $^3J_{HH}$ = 4.4 Hz, 1H, H$^{3'}$); δ(^{31}P) 19.1 (d, $^1J_{PtP}$ = 2191 Hz, $^2J_{PP}$ = 17.2 Hz, 1P, P^a atom *trans* to *κ*^{1}*C*-bipyO-H), 23.6 (d, $^1J_{PtP}$ = 1959 Hz, $^2J_{PP}$ = 17.2 Hz, 1P, P^b atom *trans* to Me); δ(^{195}Pt) -4578 (dd, $^1J_{PtP}$ = 2193 and 1968 Hz, 1Pt).

X-ray Crystallography

Single crystals of **2** were suitable for X-ray diffraction analysis and were grown by slow vapor diffusion of *n*-hexane into CH_2Cl_2 solution of this complex. X-ray intensity data were

collected using the full sphere routine by φ and ω scans strategy on the Agilent *SuperNova* dual wavelength EoS S2 diffractometer with mirror monochromated Mo *Kα* radiation (λ = 0.71073 Å). The crystal was cooled to 150 K using an Oxford Diffraction Cryojet low-temperature attachment. The data reduction, including an empirical absorption correction using spherical harmonics, implemented in *SCALE3 ABSPACK* scaling algorithm,[52] was performed using the *CrysAlisPro* software package.[53] The crystal structure was solved by direct methods using the online version of *AutoChem 2.0* in conjunction with *OLEX2* suite of programs implemented in the *CrysAlis* software.[54, 55] The non-hydrogen atoms were refined anisotropically. All of the hydrogen atoms were positioned geometrically in idealized positions and refined with the riding model approximation, with U_{iso}(H) = 1.2 or 1.5 U_{eq}(C). For the molecular graphics the program SHELXTL was used.[56] All geometric calculations were carried out using the *PLATON* software.[57]

Computational Details

Density functional theory (DFT) calculations have been performed using the *Gaussian 09* package to perform geometry optimizations, the vibrational frequencies and the electronic structures of complex **2**.[46] A frequency calculation after each geometry optimization ensured that the calculated structures are real minima in the potential energy surface of the molecules. The structure of complex **2** was optimized using the B3LYP exchange-correlation functionals with the quasirelativistic Stuttgart–Dresden (SDD) effective core pseudopotential (ECP) and corresponding set of basic functions for Pt atom and 6-31G* (five pure d functions) for C, H, N, O, and P.[58] Molecular orbital (MO) compositions and the overlap populations were calculated using the AOMix *6.88* program.[59, 60] Atomic charges were calculated using the Mulliken population analysis (MPA) as implemented in *Gaussian 09*. The analysis of the molecular orbital (MO) compositions in terms of the highest occupied orbitals and lowest unoccupied orbitals of the fragment species (HOFOs and LUFOs, respectively) and construction of orbital interaction diagrams were performed by the AOMix *6.88* program. Charge decomposition analysis (CDA) implemented in AOMix *6.88* program was used to provide better qualitative and quantitative understanding of the nature of the chemical bonding in the complex based on the electron donation and back-donation between the metal and other fragments. Excited singlet states (50 states) were calculated by time-dependent DFT (TD-DFT) in CH_2Cl_2 solvent which was described by conductor–like polarizable

continuum model (CPCM).[61] The TD-DFT output contained information for the excited-state energies and oscillator strengths (*f*) and a list of the excitations that give rise to each excited states, the orbitals involved as well as the wavefunction coefficients of the excitations. From the TD-DFT calculations the electronic distribution and the localization of the singlet excited states was visualized using the electron density difference maps (EDDMs).[62] *GaussSum3* was used for EDDMs calculations and for the electronic spectrum simulation.[63]

Electrochemistry

Cyclic voltammetry (CV) measurements were performed in a three-electrode cell using an Autolab101 potentiostat (Eco.Chemie, the Netherlands). In this system, platinum electrode and Ag/AgCl electrodes were employed as counter and reference electrodes, respectively. All complexes **1-4** and the dppf ligand were introduced into the structure of carbon paste electrode for electrochemical investigations. Cyclic voltammograms of the complexes were recorded at room temperature in acetonitrile containing 0.05 M lithium perchlorate ($LiClO_4$) as a supporting electrolyte under inert nitrogen atmosphere. The electrochemistry of [complexes **1-4** and the dppf ligand were studied in different potential windows. At first, cyclic voltammograms were recorded between +2.0 to -2.0 V at different scan rates. Then, the electrochemical properties were studied in a narrower potential window (-1.0 V to +1.0 V).

Electronic supplementary information (ESI) available: Full NMR spectra, crystallographic, electrochemistry, computational and Molecular simulation details.

Acknowledgments

This work was supported by the Institute for Advanced Studies in Basic Sciences (IASBS) Research Council and the Iran National Science Foundation (Grant no. 95822524). Collaboration of medicinal chemistry, faculty of pharmacy, Ahvaz Jundishapur University of Medical Sciences, in providing the required facilities for this work is greatly acknowledged. RK is thankful to Sharif University of Technology research Council for the research facility. PRR is grateful to the Engineering and Physical Sciences Research Council (EPSRC) for continued funding (EP/K004956/1). Thanks are also due to Mr. A. Biglari, the operator of Bruker NMR instrument at IASBS, for recording the NMR spectra.

References

1. A. Togni and T. Hayashi, *Ferrocenes: Homogeneous Catalysis, Organic Synthesis, Materials Science*, Wiley-VCH Verlag GmbH, 1995.
2. P. Štěpnička, *Ferrocenes: Ligands, Materials and Biomolecules*, John Wiley & Sons, Ltd, 2008.
3. D. A. Khobragade, S. G. Mahamulkar, L. Pospíšil, I. Císařová, L. Rulíšek and U. Jahn, *Chem. Eur. J.*, 2012, **18**, 12267-12277.
4. G. Bandoli and A. Dolmella, *Coord. Chem. Rev.*, 2000, **209**, 161-196.
5. M. Golbon Haghighi, S. M. Nabavizadeh, M. Rashidi and M. Kubicki, *Dalton Trans.*, 2013, **42**, 13369-13380.
6. S. Jamali, S. M. Nabavizadeh and M. Rashidi, *Inorg. Chem.*, 2008, **47**, 5441-5452.
7. S. M. Nabavizadeh, H. Amini, H. R. Shahsavari, M. Namdar, M. Rashidi, R. Kia, B. Hemmateenejad, M. Nekoeinia, A. Ariafard, F. Niroomand Hosseini, A. Gharavi, A. Khalafi-Nezhad, M. T. Sharbati and F. Panahi, *Organometallics*, 2011, **30**, 1466-1477.
8. S. M. Nabavizadeh, M. Dadkhah Aseman, B. Ghaffari, M. Rashidi, F. Niroomand Hosseini and G. Azimi, *J. Organomet. Chem.*, 2012, **715**, 73-81.
9. H. Samouei, M. Rashidi and F. W. Heinemann, *J. Organomet. Chem.*, 2011, **696**, 3764-3771.
10. F. Zheng, A. T. Hutton, C. G. C. E. van Sittert, W. J. Gerber and S. F. Mapolie, *Dalton Trans.*, 2015, **44**, 1969-1981.
11. S. Paziresh, R. Aghakhanpour Babadi and A. R. Esmaeilbeig, *J. Organomet. Chem.*, 2016, **803**, 73-81.
12. A. Houlton, D. M. P. Mingos, D. M. Murphy, D. J. Williams, L.-T. Phang and T. S. A. Hor, *J. Chem. Soc., Dalton Trans.*, 1993, DOI: 10.1039/dt9930003629, 3629-3630.
13. M. C. Gimeno, A. Laguna, C. Sarroca and P. G. Jones, *Inorg. Chem.*, 1993, **32**, 5926-5932.
14. A. Acosta-Ramírez, M. Muñoz-Hernández, W. D. Jones and J. J. García, *J. Organomet. Chem.*, 2006, **691**, 3895-3901.
15. O. Crespo, M. C. Gimeno and A. Laguna, *Appl. Organomet. Chem.*, 2000, **14**, 644-652.
16. F. Canales, M. C. Gimeno, P. G. Jones, A. Laguna and C. Sarroca, *Inorg. Chem.*, 1997, **36**, 5206-5211.
17. D. Giardina-Papa, I. Ara, S. Ibáñez, P. Mastrorilli, V. Gallo and J. Forniés, *Polyhedron*, DOI: http://dx.doi.org/10.1016/j.poly.2016.05.040.
18. H. R. Shahsavari, M. Rashidi, S. M. Nabavizadeh, S. Habibzadeh and F. W. Heinemann, *Eur. J. Inorg. Chem.*, 2009, 3814-3820.
19. A. Diez, J. Fernandez, E. Lalinde, M. T. Moreno and S. Sanchez, *Dalton Trans.*, 2008, DOI: 10.1039/b806572a, 4926-4936.
20. Y. Hokai, B. Jurkowicz, J. Fernández-Gallardo, N. Zakirkhodjaev, M. Sanaú, T. R. Muth and M. Contel, *J. Inorg. Biochem.*, 2014, **138**, 81-88.
21. J. F. Hartwig, *Inorg. Chem.*, 2007, **46**, 1936-1947.
22. M. Albrecht, *Chem. Rev.*, 2009, **110**, 576-623.
23. Y. Chi and P.-T. Chou, *Chem. Soc. Rev.*, 2010, **39**, 638-655.
24. I. Omae, *Cyclometalation Reactions: Five-Membered Ring Products as Universal Reagents*, Springer, 2014.

25. W.-Y. Wong and C.-L. Ho, *Acc. Chem. Res.*, 2010, **43**, 1246-1256.
26. G. Zhou, W.-Y. Wong, S.-Y. Poon, C. Ye and Z. Lin, *Adv. Funct. Mater.*, 2009, **19**, 531-544.
27. B. Butschke and H. Schwarz, *Chem. Sci.*, 2012, **3**, 308-326.
28. B. Butschke, M. Schlangen, D. Schröder and H. Schwarz, *Chem. Eur. J.*, 2008, **14**, 11050-11060.
29. A. Zucca, G. L. Petretto, S. Stoccoro, M. A. Cinellu, M. Manassero, C. Manassero and G. Minghetti, *Organometallics*, 2009, **28**, 2150-2159.
30. L. Maidich, G. Dettori, S. Stoccoro, M. A. Cinellu, J. P. Rourke and A. Zucca, *Organometallics*, 2015, **34**, 817-828.
31. M. E. Moustafa, P. D. Boyle and R. J. Puddephatt, *Organometallics*, 2014, **33**, 5402-5413.
32. M. Niazi and H. R. Shahsavari, *J. Organomet. Chem.*, 2016, **803**, 82-91.
33. A. Zucca, L. Maidich, V. Carta, G. L. Petretto, S. Stoccoro, M. Agostina Cinellu, M. I. Pilo and G. J. Clarkson, *Eur. J. Inorg. Chem.*, 2014, **2014**, 2278-2287.
34. O. Toma, N. Mercier, M. Allain, A. Forni, F. Meinardi and C. Botta, *Dalton Trans.*, 2015, **44**, 14589-14593.
35. M. Niazi and H. R. Shahsavari, *ChemistrySelect*, 2016, **1**, 1780-1783.
36. M. Niazi, H. R. Shahsavari, M. Golbon Haghighi, M. R. Halvagar, S. Hatami and B. Notash, *RSC Adv.*, 2016, **6**, 76463-76472.
37. M. Niazi, H. R. Shahsavari, M. Golbon Haghighi, M. R. Halvagar, S. Hatami and B. Notash, *RSC Adv.*, 2016, **6**, 95073-95084.
38. J. D. Scott and R. J. Puddephatt, *Organometallics*, 1983, **2**, 1643-1648.
39. M. Golbon Haghighi, M. Rashidi, S. M. Nabavizadeh, S. Jamali and R. J. Puddephatt, *Dalton Trans.*, 2010, **39**, 11396-11402.
40. L. Maidich, G. Zuri, S. Stoccoro, M. A. Cinellu and A. Zucca, *Dalton Trans.*, 2014, **43**, 14806-14815.
41. A. R. Esmaeilbeig, M. Golbon Haghighi, S. Nikahd, S. Hashemi, M. Mosarezaee, M. Rashidi and S. M. Nabavizadeh, *J. Organomet. Chem.*, 2014, **755**, 93-100.
42. R. Puttreddy, O. Jurcek, S. Bhowmik, T. Makela and K. Rissanen, *Chem. Commun.*, 2016, **52**, 2338-2341.
43. S. J. Hoseini, M. Mohamadikish, K. Kamali, F. W. Heinemann and M. Rashidi, *Dalton Trans.*, 2007, DOI: 10.1039/b700009j, 1697-1704.
44. M. Jamshidi, S. M. Nabavizadeh, H. R. Shahsavari and M. Rashidi, *RSC Adv.*, 2015, **5** 57581–57591.
45. B. J. Coe, S. P. Foxon, R. A. Pilkington, S. Sánchez, D. Whittaker, K. Clays, G. Depotter and B. S. Brunschwig, *Organometallics*, 2015, **34**, 1701-1715.
46. M. J. Frisch, G. W. Trucks, H. B. Schlegel, G. E. Scuseria, M. A. Robb, J. R. Cheeseman, G. Scalmani, V. Barone, B. Mennucci, G. A. Petersson, H. Nakatsuji, M. Caricato, X. Li, H. P. Hratchian, A. F. Izmaylov, J. Bloino, G. Zheng, J. L. Sonnenberg, M. Hada, M. Ehara, K. Toyota, R. Fukuda, J. Hasegawa, M. Ishida, T. Nakajima, Y. Honda, O. Kitao, H. Nakai, T. Vreven, J. J. A. Montgomery, J. E. Peralta, F. Ogliaro, M. Bearpark, J. J. Heyd, E. Brothers, K. N. Kudin, V. N. Staroverov, T. Keith, R. Kobayashi, J. Normand, K. Raghavachari, A. Rendell, J. C. Burant, S. S. Iyengar, J. Tomasi, M. Cossi, N. Rega, J. M. Millam, M. Klene, J. E. Knox, J. B. Cross, V. Bakken, C. Adamo, J. Jaramillo, R.

Gomperts, R. E. Stratmann, O. Yazyev, A. J. Austin, R. Cammi, C. Pomelli, J. W. Ochterski, R. L. Martin, K. Morokuma, V. G. Zakrzewski, G. A. Voth, P. Salvador, J. J. Dannenberg, S. Dapprich, A. D. Daniels, O. Farkas, J. B. Foresman, J. V. Ortiz, J. Cioslowski and D. J. Fox, *Gaussian 09, Revision B.01*, 2010.
47. S. I. Gorelsky, S. Ghosh and E. I. Solomon, *J. Am. Chem. Soc.*, 2006, **128**, 278-290.
48. S. I. Gorelsky and E. I. Solomon, *Theor. Chem. Acc.*, 2008, **119**, 57-65.
49. G. T. Burdzinski, T. L. Gustafson, J. C. Hackett, C. M. Hadad and M. S. Platz, *J. Am. Chem. Soc.*, 2005, **127**, 13764-13765.
50. K. B. Wiberg, C. M. Hadad, C. M. Breneman, K. E. Laidig, M. A. Murcko and T. J. Lepage, *Science*, 1991, **252**, 1266-1272.
51. B. S. Furniss, A. J. Hannaford, P. W. G. Smith and A. R. Tatchell, *Vogel's Textbook of Practical Organic Chemistry*, Longman Scientific & Technical, 5th edn., 1989.
52. R. C. Clark and J. S. Reid, *Acta Cryst.*, 1995, **A51**, 887-897.
53. , SuperNova Eos S2 System: Empirical absorption correction, 2011, CrysAlis-Software package, Oxford Diffraction Ltd.
54. O. V. Dolomanov, L. J. Bourhis, R. J. Gildea, J. A. K. Howard and H. Puschmann, *J. Appl. Cryst.*, 2009, **42**, 339-341.
55. , Agilent (2012): AutoChem 2.0, in conjunction with OLEX2. Agilent Technologies UK Ltd, Yarnton, Oxfordshire, England.
56. A. Spek, *Acta Cryst.*, 2009, **D65**, 148-155.
57. G. Sheldrick, *Acta Cryst.*, 2008, **A64**, 112-122.
58. D. Andrae, U. Häußermann, M. Dolg, H. Stoll and H. Preuß, *Theor. Chim. Acta*, 1990, **77**, 123-141.
59. S. I. Gorelsky and A. B. P. Lever, *J. Organomet. Chem.*, 2001, **635**, 187-196.
60. S. I. Gorelsky, AOMix program, http://www.sg-chem.net/.
61. M. Cossi and V. Barone, *J Chem Phys.*, 2001, **115**, 4708-4717.
62. W. R. Browne, N. M. O'Boyle, J. J. McGarvey and J. G. Vos, *Chem. Soc. Rev.*, 2005, **34**, 641-663.
63. N. M. O'Boyle, A. L. Tenderholt and K. M. Langner, *J. Comput. Chem.*, 2008, **29**, 839-845.